LHCb-PUB-2009-015
S. Stone
L. Zhang
Aug. 12, 2009

Measuring the CP Violating Phase in B_s Mixing Using $B_s^0 \to J/\psi f_0(980)$

Abstract

We show that the decay $B_s^0 \to J/\psi f_0(980)$, $f_0(980) \to \pi^+\pi^-$ can be used to measure the CP violating phase in B_s mixing, $-2\beta_s$, and estimate the sensitivity as ± 0.050 rad, for 2 fb^{-1} of LHCb data. After adding in the related $B_s^0 \to J/\psi\eta'$, $\eta' \to \rho\gamma$ mode, the sensitivity improves to ± 0.044 rad. Use of these CP eigenstates obviates the need for a transversity analysis that must be used in the case of $B_s^0 \to J/\psi\phi$ decays.

1 Introduction

While CP violation in B^0 decays has been measured unequivocally, attempts at determining the CP violating phase in B_s mixing, $-2\beta_s$ [1] by the CDF and D0 experiments using $B_s^0 \to J/\psi\phi$ decays [2], have given values much larger than Standard Model (SM) predictions, but with large enough errors that the measurements are not statistically significant, even when combined [3]. Since this mode is not a CP eigenstate, but one involving two vector particles an angular analysis is necessary [4]. These analyses, however, did not allow for the possibility of there being an S-wave component in the ϕ mass region, thus possibly biasing the result and surely underestimating the error [5].

Since physics beyond the SM can or even should contribute virtual particles that interfere in the B_s mixing loop, it is important to measure the mixing phase as precisely and in an unbiased manner as possible. It has long been known that the modes $B_s^0 \to J/\psi\eta^{(\prime)}$ are CP eigenstates, and thus angular analysis is not needed. All of the η or η' decay modes contain at least one photon, whose reconstruction is much less efficient than charged particles in LHCb. One study has estimated the sensitivity using $\eta' \to \rho\gamma$ [6], but the sensitivity is of the order of a factor of two worse than that expected using $J/\psi\phi$ mode. Other modes have also been considered [7].

In this note we describe the event selection, the backgrounds, and make an estimate of the measurement sensitivity of $-2\beta_s$, using a heretofore not considered mode $B_s^0 \to J/\psi f_0(980)$, where $f_0(980) \to \pi^+\pi^-$. The dominant Feynman diagrams for the ϕ and f_0 processes are shown in Fig. 1. There also are possible small contributions from penguin diagrams [8] and W-exchange [9].

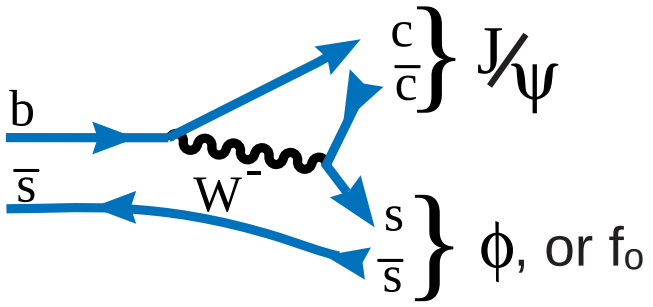

Figure 1: Decay diagrams for $B_s \to J/\psi\phi$, and $B_s \to J\psi f_0$.

There have been several estimates of the relative widths of these decay modes. Based on studies of hadronic D_s^+ decays Stone and Zhang [5] estimate that the relative width is

$$R_{f/\phi} \equiv \frac{\Gamma(B_s^0 \to J/\psi f_0,\ f_0 \to \pi^+\pi^-)}{\Gamma(B_s^0 \to J/\psi\phi,\ \phi \to K^+K^-)} \approx 20\% \ . \tag{1}$$

There also is a non-f_0 $\pi^+\pi^-$ S-wave component that is very wide in mass, and contributes an additional 5% of the $J/\psi\phi$ rate using a narrow selection of ± 90 MeV around the f_0 mass that was used in the sensitivity estimate [5].

Recently, the CLEO collaboration [10] has reported another estimate of $R_{f/\phi}$ using measurements of the semileptonic widths of $D_s^+ \to f_0 e^+\nu$ and $D_s^+ \to \phi e^+\nu$ at the endpoint of the four-momentum transfer range where the phase space is maximum, as suggested by Stone and Zhang. These measurements yield

$$R_{f/\phi} \equiv \frac{\frac{d\Gamma}{dq^2}(D_s^+ \to f_0(980) e^+\nu,\ f_0 \to \pi^+\pi^-)\mid_{q^2=0}}{\frac{d\Gamma}{dq^2}(D_s^+ \to \phi e^+\nu,\ \phi \to K^+K^-)\mid_{q^2=0}} = (42 \pm 11)\% \ . \tag{2}$$

A note on notation, since it is clumsy to always refer to $-2\beta_s$ we set this equal to ϕ_f to indicate that this is the CP violating phase measured in $B_s \to J/\psi f_0$ decays, which should to an excellent approximation be the same phase as measured in $B_s \to J/\psi\phi$ decays even in the presence of new physics in the mixing amplitude.

2 Signal Selection and Optimization

The present study is done using a Monte Carlo simulation of the signal and specific backgrounds. For the signal, a B_s is produced in a 14 TeV proton proton collision conforming to the theoretical fragmentation function. It is allowed to decay and the quasi-stable particles then traverse the detector where they are subject to magnetic fields, multiple scattering in material, decays and hadronic interactions [11]. To optimize the selection, we generate a signal sample, and several background samples. We use a generic $pp \to J/\psi\ X$ sample to predict the backgrounds when we have a J/ψ present in the event, though these events should be eliminated since the J/ψ is produced at the primary vertex (PV). To study the background from b decays we use a generic

b decay sample that also includes $b \to J/\psi\ X$ decays. However, some individual modes present specific problems, so we also generate them separately. Table 1 lists the different decay channels that have been generated, the number of analyzed events passing the geometrical cuts, and the geometrical cut efficiencies.

We first generate the events and pre-select the ones within the geometrical acceptance: for exclusive b decays we insist that the charged B candidate decay tracks are below 400 mrad and larger than 10 mrad with respect to the beam line. In the case of the inclusive J/ψ sample, we insist only that both muon tracks pass the above mentioned criteria. For the inclusive $b\bar{b}$, we only require that the one of the two B mesons be pointed within 400 mrad of the beam line.

Table 1: MC samples used in this study.

Decay	Number of events	Geometrical cut efficiency
$B_s^0 \to J/\psi(\mu\mu)f_0(\pi\pi)$	60,565	16.4%
$B_d^0 \to J/\psi(\mu\mu)K^{*0}(K\pi)$	2,994,516	17.3%
$B_u^+ \to J/\psi(\mu\mu)K^+$	1,928,159	17.9%
$B_s^0 \to J/\psi(\mu\mu)\eta'(\rho\gamma)$	63,319	16.4%
$B_u^+ \to J/\psi(\mu\mu)X$	2,831,431	20.4%
$B_d^0 \to J/\psi(\mu\mu)X$	2,924,276	20.4%
$B_s^0 \to J/\psi(\mu\mu)X$	720,109	20.2%
inclusive $J/\psi(\mu\mu)$	4,237,046	19.7%
inclusive $b\bar{b}$	20,176,844	43.7%

Table 2 lists the production cross sections at 14 TeV predicted by Pythia/EvtGen, used in our Monte Carlo simulation.[1]

Table 2: Production cross sections at 14 TeV predicted by Pythia/EvtGen, used in our Monte Carlo simulation. The double arrow (i.e. $\Rightarrow$) indicates the existence of possible intermediate states, e.g. $\sigma_{pp\Rightarrow J/\psi X}$ includes $\sigma_{pp\to b\to J/\psi X}$. The "prompt J/ψ" cross section is $\sigma_{\text{prompt } J/\psi} = \sigma_{pp\to J/\psi X} - \sigma_{pp\to b\Rightarrow J/\psi X}$ =0.266 mb.

cross section	mb
σ_{pp}	102.9
$\sigma_{pp\to b\bar{b}}$	0.698
$\sigma_{pp\Rightarrow J/\psi X}$	0.286
$\sigma_{pp\to b\Rightarrow J/\psi X}$	0.0204

To reconstruct the $J/\psi f_0$ ($J/\psi \to \mu^+\mu^-$, $f_0 \to \pi^+\pi^-$) candidates, we first insist that we have two opposite sign muon candidates that form a J/ψ candidate and satisfy the "pre-selection" criteria listed in Table 3. Then we require two additional charged tracks, that satisfy other loose-pre-selection cuts, and are consistent with making a vertex with the two muons. The very loose pre-selection criteria are chosen with the aim to remove as little signal as possible, and reject large parts of the combinational background. This pre-selection is also applied to inclusive $b\bar{b}$ and inclusive J/ψ events.

[1]We kept the LHC energy at 14 TeV in order to compare with other simulations involving ϕ_f. For 10 TeV running, the final signal yields should be scaled by a factor of $\approx$5/7.

Table 3: Cut values for the $B_s^0 \to J/\psi f_0$ pre-selection and selection. Also shown are the selection efficiency of each cut for the signal (absolute) and background (with respect to "pre-selection.") $\Delta\mathcal{L}_{ij}$ is the likelihood ratio of species i relative to species j. The product of the p_T values of J/ψ daughters is used to help eliminate any residual minimum bias background.

Cuts on the muons	Pre-Selection	Selection	signal efficiency(%)	BG efficiency(%)
$\Delta\mathcal{L}_{\mu\pi}$	> -5	> -5	97.2	-
$\chi^2_{\rm track}$/nDof	-	< 5	98.9	85.9
Cuts on the J/ψ				
Product $p_{\rm T}$ of daughters	-	$> 500^2$ MeV^2	100	100
Mass Window	± 42 MeV	± 42 MeV	97.9	-
Cuts on the pions				
$\Delta\mathcal{L}_{\pi K}$	> -10	> -10	99.2	-
$\Delta\mathcal{L}_{\pi\mu}$	> -10	> -10	99.9	-
$\chi^2_{\rm track}$/nDof	-	< 4	95.3	65.2
Min IPS	-	> 3	74.8	1.5
Cuts on the $f_0(980)$				
Sum $p_{\rm T}$ of daughters	-	> 900 MeV	98.6	57.6
Mass Window	± 500 MeV	± 90 MeV	-	-
Cuts on the B_s^0				
Max IPS	-	< 5	99.7	67.5
vertex fit χ^2	< 50	< 17	88.1	51.8
$\cos\theta_p$	-	> 0.99993	80.4	4.8
Mass Window	± 300 MeV	± 50 MeV	98.5	-

2.1 $J/\psi \to \mu^+\mu^-$ selection

Muon candidates are selected by requiring the track has hits in the Muon Chambers and satisfies the identification criterion that requires global $\Delta\mathcal{L}_{\mu\pi} > -5$, and has $\chi^2_{\rm track}$ per # of degrees of freedom (nDOF) of the Kalman fit of the track < 5 (Fig. 2 (d)). Specifically, $\Delta\mathcal{L}_{p_1p_2}$ is the difference in the log of the likelihood between the hypothesis that this particle is of type of p_1 rather than p_2 (equivalent to the likelihood ratio). These cuts were studied in Ref. [12] using minimum bias events and are aimed at rejecting hadrons misidentified as muons due to random combinations of spurious hits in the Muon Chambers. The distributions of transverse momentum ($p_{\rm T}$) for μ^+ vs. μ^-, the minimum impact parameter significance (IPS) with respect to each primary vertex,[2] $\chi^2_{\rm track}$/nDOF and momentum of muon candidates are shown in

[2]The Impact Parameter Significance is defined as the track impact parameter with respect to a primary vertex divided by its error: IPS $\equiv$ $(\frac{\rm IP}{\sigma_{\rm IP}})$. At the luminosity of 2×10^{-32} cm^{-2}s^{-1} about 35% of the events have

Fig. 2(a-e) from the signal and inclusive $b\bar{b}$ MC after "pre-selection."

We then combine two opposite sign muon candidates to form a J/ψ candidate. Fig. 3 shows the signal and $b\bar{b}$ distributions for IPS, the flight distance significance (the distance from PV to reconstruction vertex divided by its error), the vertex fit χ^2 and invariant mass of J/ψ candidates from the signal and inclusive $b\bar{b}$ MC after "pre-selection." We retain those events having $|m_{\mu\mu} - m_{J/\psi}| < 42$ MeV corresponding to about a $\pm 3\sigma$ interval (Fig. 3 (d)). These selections result in a relatively clean J/ψ sample.

2.2 $f_0(980) \to \pi^+\pi^-$ selection

To select pion candidates we veto tracks identified as kaons with $\Delta\mathcal{L}_{K\pi} > 10$ or muons with $\Delta\mathcal{L}_{\mu\pi} > 10$. The veto has $> 99\%$ efficiency for signal. Fig. 4 shows the distributions of $p_{\rm T}$ for π^+ vs. π^-, the minimum IPS with respect to each primary vertex, $\chi^2_{\rm track}$/nDOF and momentum of pion candidates from the signal and inclusive $b\bar{b}$ MC after "pre-selection."

We then combine two opposite sign pion candidates to form a $f_0(980)$ candidate. Fig. 5 shows the minimum IPS, flight significance, and vertex χ^2 distributions for $f_0(980)$ candidates from the signal and inclusive $b\bar{b}$ samples after "pre-selection."

2.3 B_s^0 reconstruction

A B_s^0 is reconstructed by combining J/ψ and $f_0(980)$ candidates. We require the four tracks from J/ψ and $f_0(980)$ to be consistent with coming from one vertex as evaluated by examining the vertex fit χ^2, where the nDOF is 5. We also calculate the cosine of the angle between the B_s^0 candidates reconstructed momentum and direction from the primary vertex to B_s^0 vertex ($\cos\theta_p$), Fig. 6 shows the distributions of B_s^0 candidates from the signal and inclusive $b\bar{b}$ MC after "pre-selection."

2.4 Optimization Criteria

To study how the ϕ_f sensitivity depends on the signal statistics (S) and the background to signal ratio (B/S), we use a fast stimulation or "Toy" Monte Carlo.

We generate and fit 400 "experiments" as a function of the B/S ratio, using ϕ_f set to its predicted SM value of -0.0368. For each B/S point we fit the resulting ϕ_f distribution to a Gaussian. (This is the same fitter as used in section 6.) The r.m.s. width (σ) of the Gaussian is taken as the ϕ_f sensitivity. For our first point we fix B/S at zero and change only the amount of signal. Fig. 7 shows the error of ϕ_f (σ_{ϕ_f}) as a function of signal yield. The curve follows the expected behavior: $\sigma_{\phi_f} \propto 1/\sqrt{S}$. To understand the relation between σ_{ϕ_f} and B/S, we fix S and only change B/S. Fig. 8 shows the the error of ϕ_f (σ_{ϕ_f}) as a function of B/S, where the experiment contains signal and a long-lived background, with a lifetime fixed at 0.96 ps, as obtained from $B \to J/\psi X$ Monte Carlo. We fit the data with a shape $\sigma_{\phi_f} \propto \sqrt{1 + \alpha \times B/S}$. The value of α is 0.63±0.10, consistent with the ratio of background lifetime to B_s lifetime, 0.64. For an exponential proper time distribution the lifetime can be quickly estimated using the mean of the distribution. For convenience we take α as the ratio

more than one primary vertex, and we choose the smallest IPS.

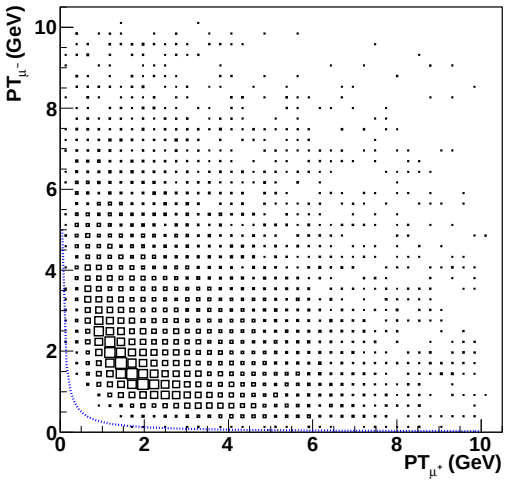

(a) $p_{\mathrm{T}}(\mu^+)$ vs $p_{\mathrm{T}}(\mu^-)$ -signal

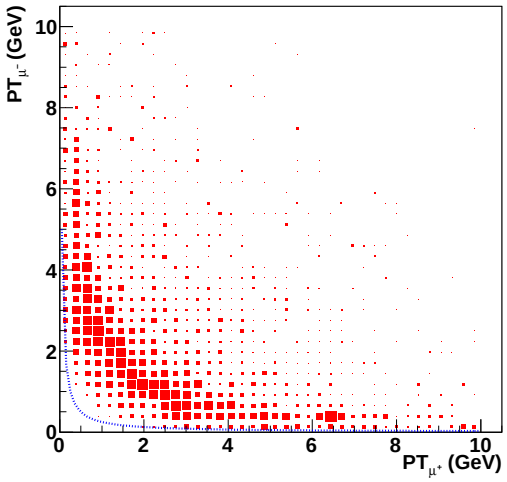

(b) $p_{\mathrm{T}}(\mu^+)$ vs $p_{\mathrm{T}}(\mu^-)$ -background

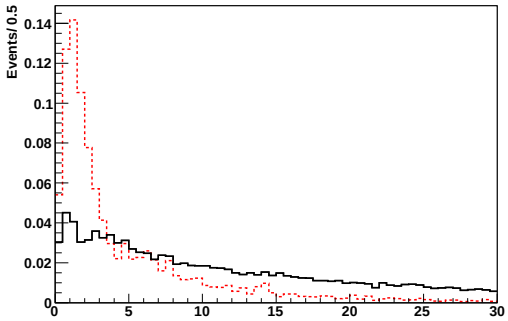

(c) Minimum IPS of muons

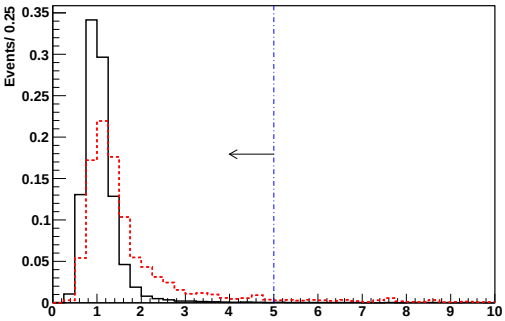

(d) χ^2_{track}/nDOF of muons

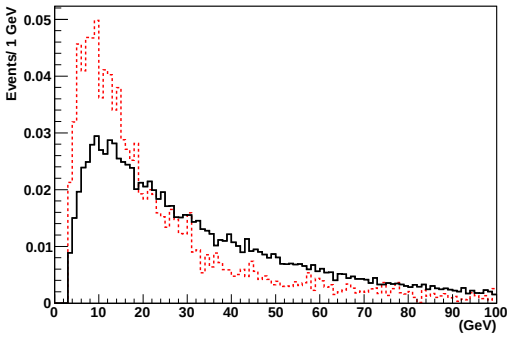

(e) Momentum of muons

Figure 2: The distributions of the signal (black solid) and $b\bar{b}$ background (red dashed) for muon candidates from J/ψ. The curves in (a) and (b) show the product of $p_{\mathrm{T}}(\mu^+) \cdot p_{\mathrm{T}}(\mu^-) = 500^2$ MeV^2, used to eliminate minimum bias events in the preselection. The final cut in (d) is indicated by vertical blue dotted lines.

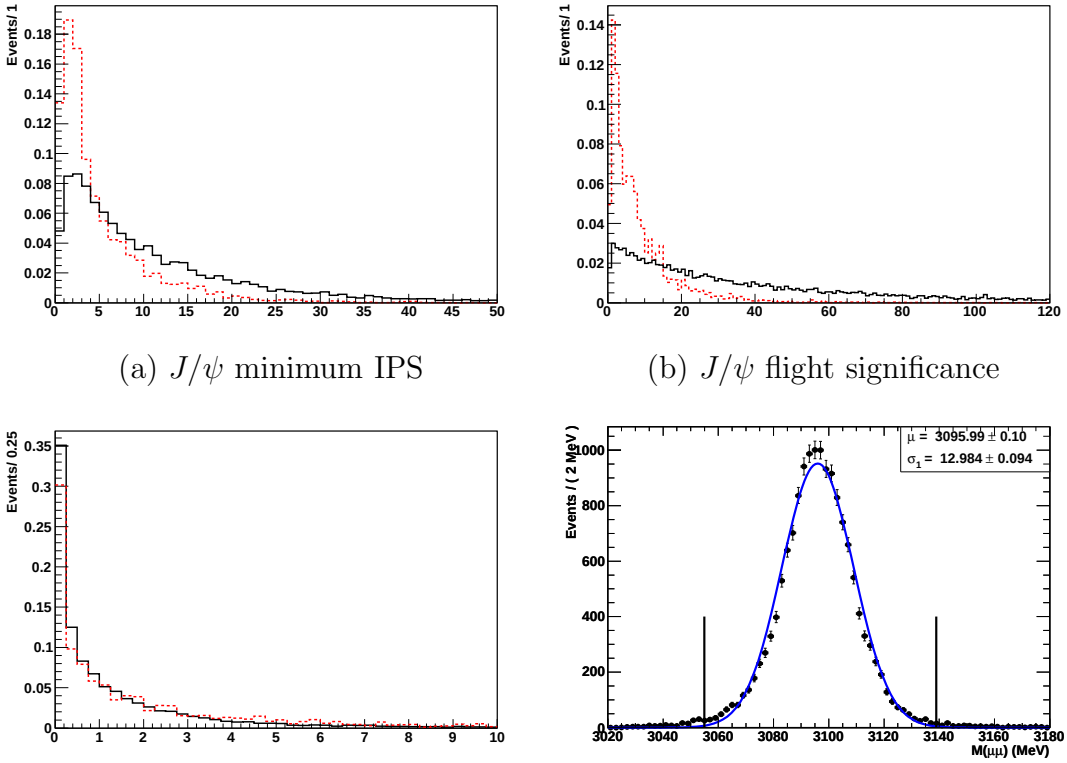

(a) J/ψ minimum IPS

(b) J/ψ flight significance

(c) J/ψ vertex χ^2

(d) J/ψ mass

Figure 3: (a)-(c): The distributions of signal (black solid) and $b\bar{b}$ background (red dashed) for J/ψ candidates. (Numbers of events in the B and S distributions are equal.) (d) The J/ψ mass distribution for signal, fit to a single Gaussian, with the selection cut indicated by vertical lines.

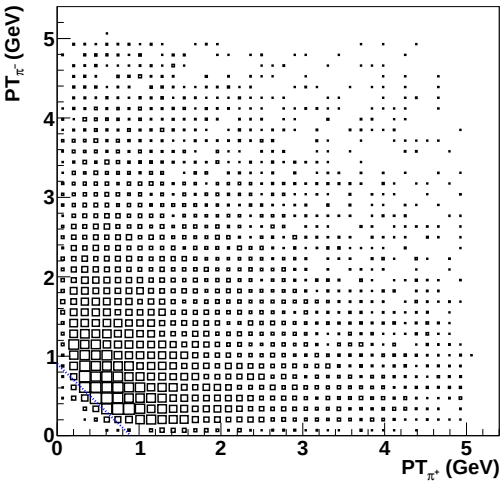

(a) $p_{\rm T}(\pi^+)$ vs $p_{\rm T}(\pi^-)$ -signal

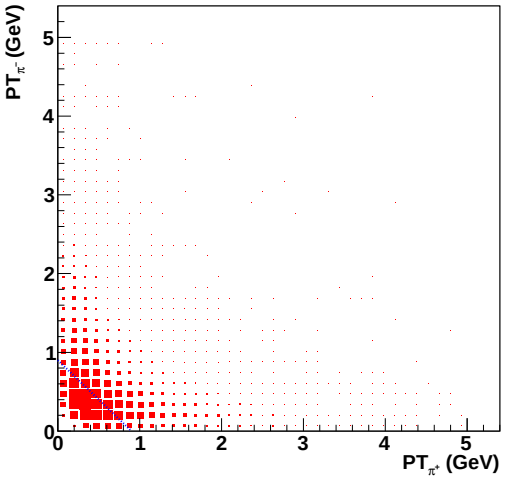

(b) $p_{\rm T}(\pi^+)$ vs $p_{\rm T}(\pi^-)$ -background

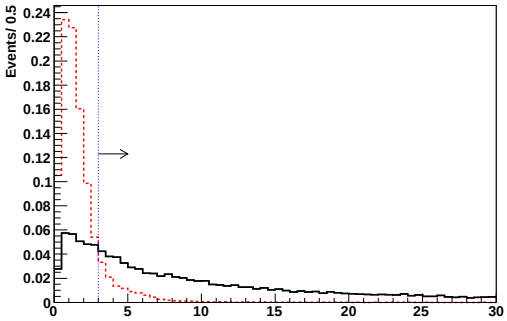

(c) Minimum IPS of pions

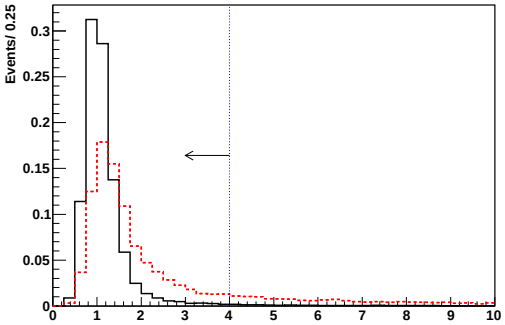

(d) $\chi^2_{\rm track}$/nDOF of pions

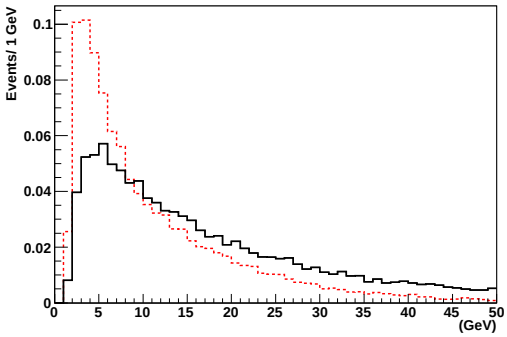

(e) Momentum of pions

Figure 4: The distributions of signal (black solid) and $b\bar{b}$ background (red dashed) for pion candidates from f_0. The final cuts in (a)-(d) are indicated by blue dotted lines. (The number of events in the B and S distributions are equal.)

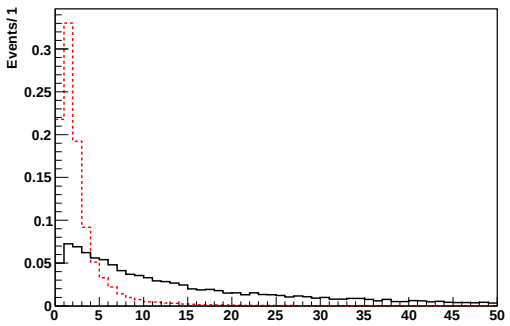

(a) f_0 minimum IPS

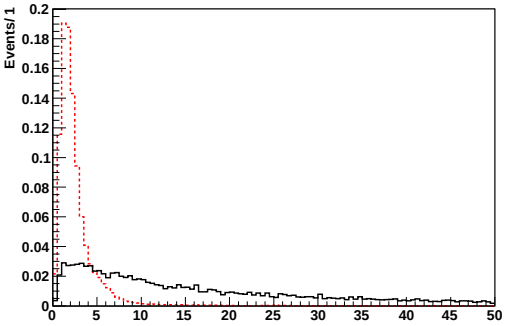

(b) f_0 flight significance

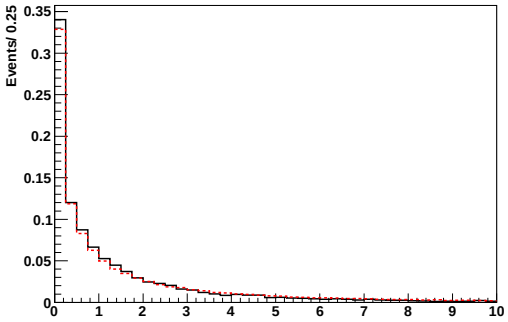

(c) f_0 vertex χ^2

Figure 5: The distributions of signal (black solid) and $b\bar{b}$ background (red dashed) for $f_0(980)$ candidates. (The number of events in the B and S distributions are equal.)

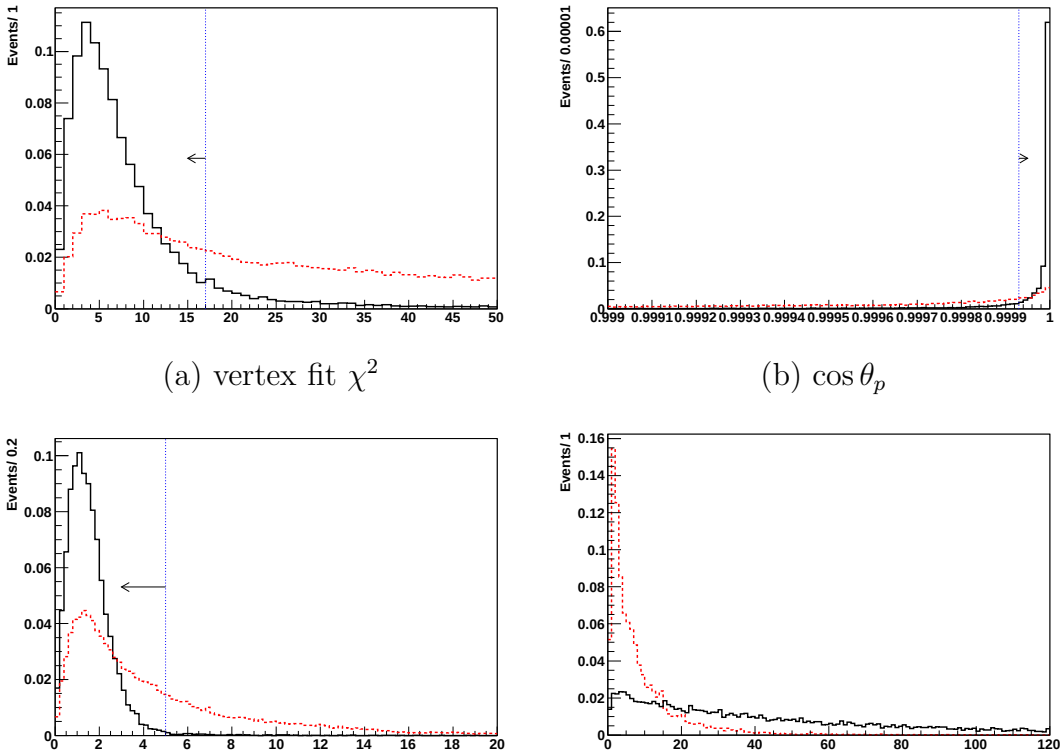

(a) vertex fit χ^2

(b) $\cos\theta_p$

(c) IPS

(d) Flight significance

Figure 6: The distributions of the signal (black solid) and $b\bar{b}$ background (red dashed) for B_s^0 candidates. Final cuts on (a)-(c) are indicated by vertical blue dotted lines.

of mean values of the proper-time distributions of background and signal. (We have also found that the ϕ_f uncertainty due to the prompt J/ψ background follows this formula.)

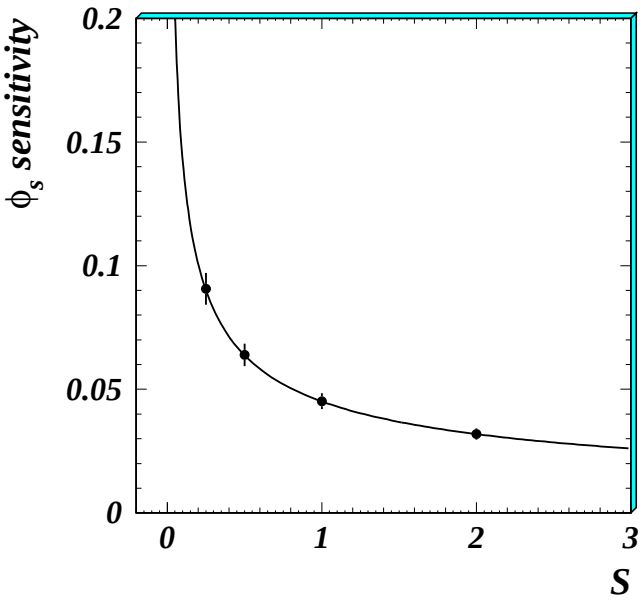

Figure 7: The error of ϕ_f as a function of signal number S. (S equal to one corresponds to about 2 fb^{-1} data.) The curve is the result of a fit to $\sigma_{\phi_f} \propto 1/\sqrt{S}$.

2.5 Selection Optimization

Our goal is to maximize the ϕ_f sensitivity. Specifically, the selection cuts are chosen to maximum $\frac{S}{\sqrt{S+\alpha \cdot B}}$ where S (B) is the expected signal (background) number within a ± 50 MeV mass window around the B_s^0 nominal mass [13], and α is the ratio of the mean values of the proper-time distributions between the background and the signal. The cuts are based on a set of variables that show a marked difference between signal versus background. They include: (1) sum of absolute $p_{\rm T}$ of f_0 daughters (Fig. 4 (a,b)); (2) impact parameter significance of pions (Fig. 4 (c)); (3) track fit $\chi^2_{\rm track}$/nDOF of pions (Fig. 4 (d)); (4) vertex fit χ^2 of $\mu^+\mu^-\pi^+\pi^-$ (Fig. 6 (a)); and (5) the cosine of the angle between the B_s^0 candidates reconstructed momentum and its flight direction ($\cos\theta_p$) (Fig. 6 (b)). (We have not explored optimizing the selection based on a neural network or similar procedure as the tuning of such a method must be based on real data, and here we are trying to understand the sensitivity to first order. If other variables also have some discrimination power between signal and background, we will include them in the future.)

In what follows, we normalize all the yields to 2 fb^{-1} data. We use the expected $b\bar{b}$ production cross-section $\sigma_{b\bar{b}} = 500$ μb and $\sigma_{\rm prompt\ J/\psi} = 265.6$ μb as predicted by Pythia, and listed in Table 2. Since the Monte Carlo used 698 μb as the $b\bar{b}$ production cross-section, we scale the number of background events from $b\bar{b}$ to the value corresponding to $\sigma_{b\bar{b}} = 500$ μb. To have more

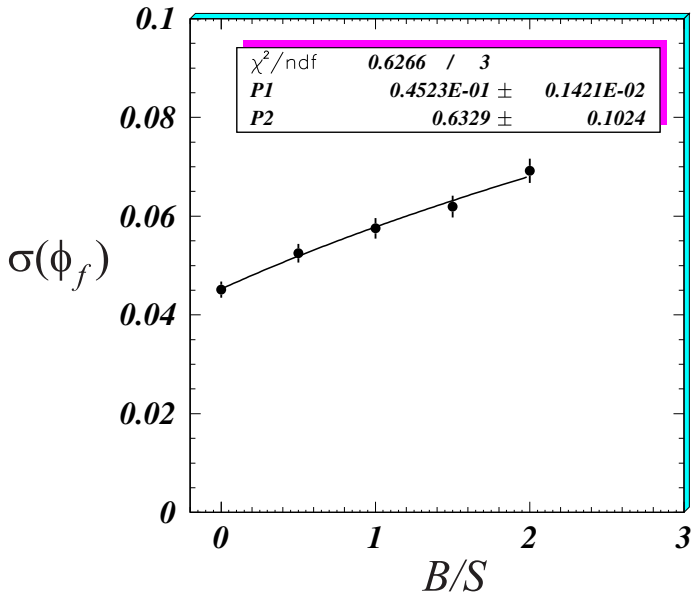

Figure 8: The error of ϕ_f as a function of background to signal ratio B/S for a fixed S. The S corresponds to about 2 fb^{-1} data. The curve shows a fit to $\sigma_{\phi_f} = A\sqrt{1+\alpha \times B/S}$. Here $\alpha \equiv P2$ and $A \equiv P1$.

statistics in the background estimation, we enlarge the f_0 window from the nominal 90 MeV to 500 MeV, and the B_s^0 window from 50 MeV to 300 MeV. If the background is distributed linearly in the larger windows, we can scale the background number in the larger windows down by a factor of 33. The factor α may change among cut variables, so we obtain α from the signal and background proper-time distributions at each set of cut points. (We regard this as a minor point, and first analyses are likely to use a fixed value of α.)

We realize that the lower mass region contains a large $B^0 \to J/\psi K^{*0}$ sample when the kaon is misidentified as a pion (see Fig. 11a); there is also a small $B_d^0 \to J/\psi\pi^+\pi^-$ background (see Fig. 9), so we remove this background from the calculation of B as we will consider this background separately. The final cuts, called "Selection," are shown in the third column of Table 3.

A selection cut of 900 MeV on $p_{\rm T}(\pi^+) + p_{\rm T}(\pi^-)$ serves to eliminate 42.4% of of the background, costing only 1.4% of the signal efficiency.

3 Signal efficiency and event yields

Table 4 shows the efficiencies computed for $B_s^0 \to J/\psi f_0$, where:

- $\epsilon_{\rm geo}$ is the efficiency of the acceptance cut at generator level on the B_s^0 daughters between 10 to 400 mrad;

- $\epsilon_{\rm det/geo}$ is the efficiency of that all B_s^0 decay products in the event are reconstructible (has enough MC hits for long track reconstruction) ;
- $\epsilon_{\rm rec/det}$ is the efficiency that the reconstructible events are actually reconstructed.
- $\epsilon_{\rm sel/rec}$ is the efficiency that the reconstructed events are actually selected.
- ϵ_{L0}, ϵ_{HLT1}, and ϵ_{HLT2} are respective efficiencies for the L0, HLT1 and HLT2 trigger algorithms.

Table 4: Efficiency for $B_s^0 \to J/\psi f_0(980)$. L0, HLT1 and HLT2 refer to the three trigger steps.

$\epsilon_{\rm geo}$ [%]	$\epsilon_{\rm det/geo}$ [%]	$\epsilon_{\rm rec/det}$ [%]	$\epsilon_{\rm sel/rec}$ [%]	$\epsilon_{\rm L0}$ [%]	$\epsilon_{\rm HLT1}$ [%]	$\epsilon_{\rm HLT2}$ [%]	$\epsilon_{\rm tot}$ [%]
16.4	38.7	71.4	45.4	94.0	95.0	95.0	1.75

The overall trigger efficiency is 85%, for signal events with all decay products inside the detector. This is a high efficiency, especially compared with fully hadronic events, which are typically at least a factor of two lower. The total efficiency including HLT2 is the product of the individual efficiencies listed above, which is 1.75%. The yield for a decay channel is computed as

$$Y = L_{\rm int} \times \sigma_{b\bar{b}} \times 2 \times f_{B_s} \times \mathcal{B}^{\rm vis} \times \epsilon_{\rm tot}, \tag{3}$$

where $L_{\rm int} = 2$ fb^{-1} is the assumed integrated luminosity, $\sigma_{b\bar{b}} = 500$ μb is the expected $b\bar{b}$ production cross-section, $f_{B_s} = (11.0 \pm 1.2)\%$ is the probability for a b-quark to form a B_s meson, and $\mathcal{B}^{\rm vis}$ is the total visible branching fraction, the product of all the individual branching fractions involved in the decay chain. (The factor of 2 arises because we can use either the b or $\overline{b}$ quark.) Assuming that $\mathcal{B}(B_s^0 \to J/\psi f_0) \times \mathcal{B}(f_0 \to \pi^+\pi^-)$ is quarter of $\mathcal{B}(B_s^0 \to J/\psi\phi) \times \mathcal{B}(\phi \to K^+K^-)$, we have $\mathcal{B}^{\rm vis}(B_s^0 \to J/\psi(\mu\mu)f_0(\pi\pi)) = 6.8 \times 10^{-6}$. After applying the efficiencies, we expect 26.1k signal events after HLT2. Table 5 shows the branching and b-hadron production fractions assumed in the calculation of the yields and background levels discussed below.

Table 5: Branching and b-hadron production fractions assumed in the calculation of the yields and background levels.

Branching fraction	value	estimated from	Ref.
$\mathcal{B}^{\rm vis}(B_s^0 \to J/\psi(\mu\mu)f_0(\pi\pi))$	6.8×10^{-6}	$B_s^0 \to J/\psi\phi$	[5]
$\mathcal{B}^{\rm vis}(B_s^0 \to J/\psi(\mu\mu)\eta'(\rho\gamma))$	10×10^{-6}	$B_d^0 \to J/\psi K^0$	[14]
$\mathcal{B}^{\rm vis}(B_d^0 \to J/\psi(\mu\mu)K^{*0}(K\pi))$	$(5.25 \pm 0.24) \times 10^{-5}$		PDG08 [13]
$\mathcal{B}^{\rm vis}(B_u^+ \to J/\psi(\mu\mu)K^+)$	$(5.9 \pm 0.2) \times 10^{-5}$		PDG08 [13]
f_u	$(39.9 \pm 1.2)\%$		PDG08 [13]
f_d	$(39.9 \pm 1.2)\%$		PDG08 [13]
f_s	$(11.0 \pm 1.2)\%$		PDG08 [13]

4 Background Sources

4.1 Prompt J/ψ

We use Monte Carlo corresponding to a 0.00125 fb^{-1} data sample and find 69 candidates passing the selection which are from prompt J/ψ events in the enlarged f_0 and B_s^0 mass regions, before applying the trigger selections. From prompt J/ψ events we expect $B/S = (11 \pm 1)\%$, where the error reflects only the uncertainty due to Monte Carlo statistics.

4.2 Background from $b\overline{b}$

Our Monte Carlo simulation used $\mathcal{B}(b \to J/\psi X)$=1.46% (see Table 2), compared with the PDG value of $(1.16 \pm 0.10)\%$ [13]. Using the Monte Carlo value, we expect $B/S = (26 \pm 2)\%$ from $b\bar{b}$ background, where the error is only the statistical uncertainty from the Monte Carlo. This is reduced to $(20 \pm 2)\%$ using the PDG value. For the purpose of this note we will use the larger value, as that was what was used in previous studies of $J/\psi\phi$. We discuss specific background sources below.

4.2.1 $B_{u,d,s} \to J/\psi X$

Fig. 9 shows the $\mu^+\mu^-\pi^+\pi^-$ invariant mass distribution from $B_{u,d,s} \to J/\psi X$. Fig. 10 shows the $m_{\pi\pi}$ distribution in the B_s^0 mass signal region.

4.2.2 $B_d^0 \to J/\psi K^{*0}$

When the kaon is misidentified as a pion, $B_d^0 \to J/\psi K^{*0}$ decay can fake a $B_s \to J/\psi\pi^+\pi^-$ event. Fig. 11 shows the invariant mass distributions for B_s^0 and f_0 candidates from $B_d^0 \to J/\psi K^{*0}$ decays. If the mass resolution does not deteriorate, we will see almost no events from this source; quantitatively, in 2 fb^{-1} of data, we expect < 10 events at 90% confidence level (C.L.) remaining in the f_0 and B_s^0 narrow signal regions.

4.2.3 $B_u^+ \to J/\psi K^+$

The $B_u^+ \to J/\psi K^+$ decay can fake a $J/\psi\pi^+\pi^-$ when the K^+ is misidentified as pion and a random π^- is combined. Fig. 11 shows the invariant mass distributions for B_s^0 and f_0 from $B_u^+ \to J/\psi K^+$ decays. We expect $(1.29 \pm 0.08) \times 10^3$ events contribute to the background before the trigger in 2 fb^{-1} data.

4.2.4 $B_s^0 \to J/\psi\eta'$

We have studied $\eta' \to \eta\pi^+\pi^-$ and $\eta' \to \rho\gamma$ and found only the latter could contribute as background. It is a dangerous background, because $B_s^0 \to J/\psi\eta'$ has opposite CP to the signal. Fig. 13 shows the invariant mass distributions for B_s^0 and f_0 from $B_s^0 \to J/\psi\eta'$, $\eta' \to \rho\gamma$ decays. Assuming $\mathcal{B}(B_s^0 \to J/\psi\eta') = \frac{2}{3}\ \mathcal{B}(B^0 \to J/\psi K^0)$ [14], we expect $(0.75 \pm 0.07) \times 10^3$ events contribute to the background, before the trigger, in 2 fb^{-1} data. Most of these, however, are not in the narrow signal mass ranges.

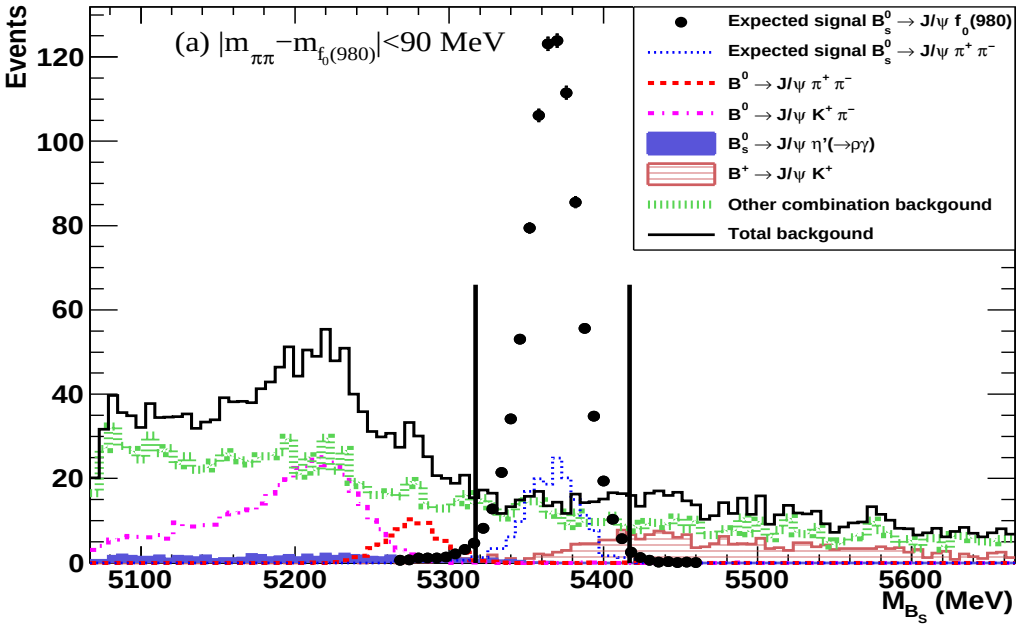

(a) $|m_{\pi\pi} - m_{f_0(980)}| < 90$ MeV

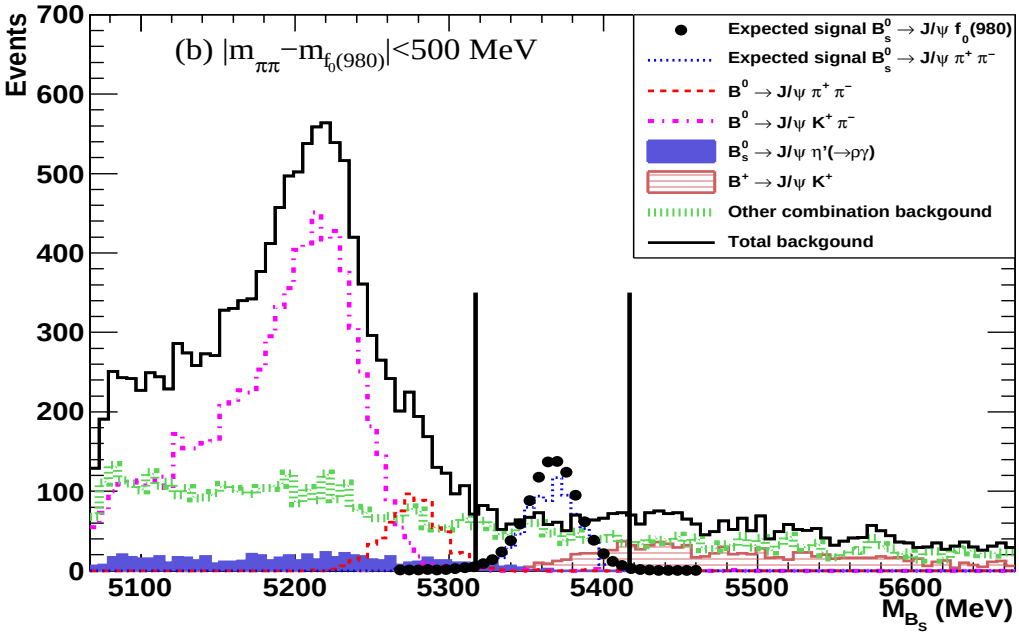

(b) $|m_{\pi\pi} - m_{f_0(980)}| < 500$ MeV

Figure 9: $\mu^+\mu^-\pi^+\pi^-$ invariant mass distributions from $B_{u,d,s} \to J/\psi X$ MC sample in (a) ± 90 MeV and (b) ± 500 MeV windows around the $f_0(980)$ nominal mass. The expected signal distributions are superimposed. The non-resonant $B_s^0 \to J/\psi\pi^+\pi^-$ branching fraction in this MC generation is set to 2×10^{-4}, about 30% of that of $B_s^0 \to J/\psi\phi, \phi \to K^+K^-$.

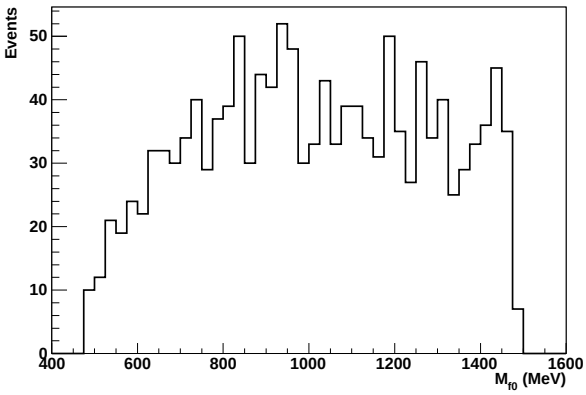

Figure 10: The $m_{\pi\pi}$ distribution in B_s^0 mass signal region ($|m_{\mu\mu\pi\pi} - m_{B_s^0}| < 50$ MeV) from the sample including all B decays with J/ψ candidates, except signal.

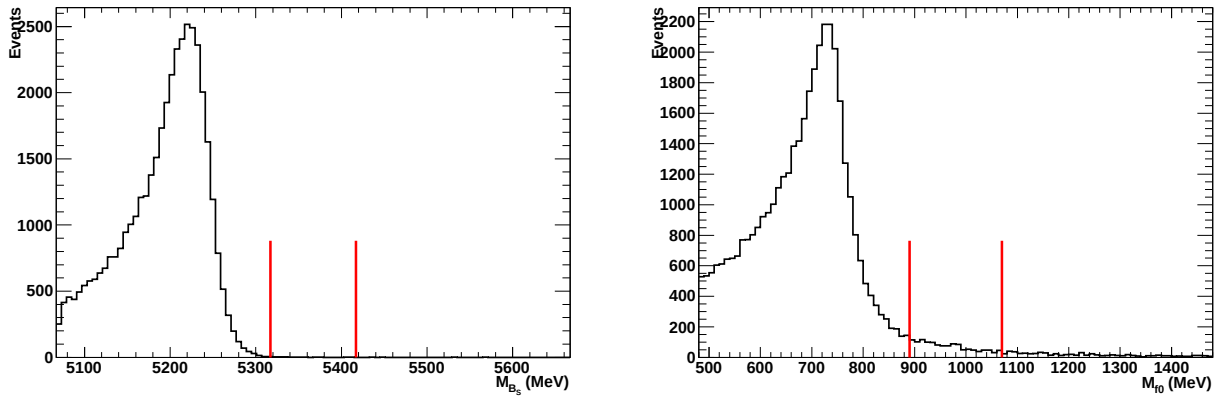

(a) $m_{\mu\mu\pi\pi}$ (b) $m_{\pi\pi}$

Figure 11: Distributions from $B_d^0 \to J/\psi K^{*0}$ decays when the kaon is misidentified as a pion. The vertical lines show the narrow mass windows.

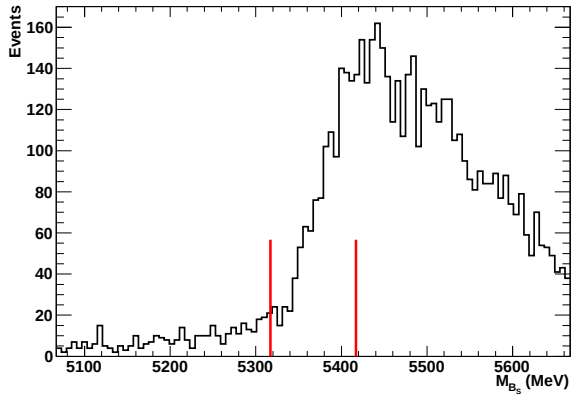

(a) $m_{\mu\mu\pi\pi}$

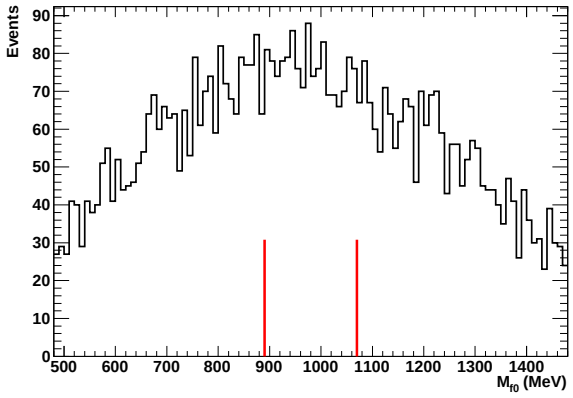

(b) $m_{\pi\pi}$

Figure 12: Distributions from $B_u^+ \to J/\psi K^+$ decays where the K^+ is misidentified as pion and a random π^- is combined. The vertical lines show the narrow mass windows.

We also intend to reconstruct these events when we can find the photon from the $\eta' \to \rho\gamma$ decay to use in a separate measurement of ϕ_f (see Sec. 6.4). We have not vetoed these events in our $J/\psi f_0$ selection, in this study.

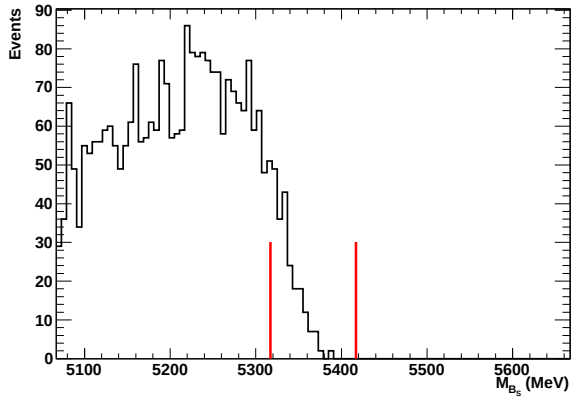

(a) $m_{\mu\mu\pi\pi}$

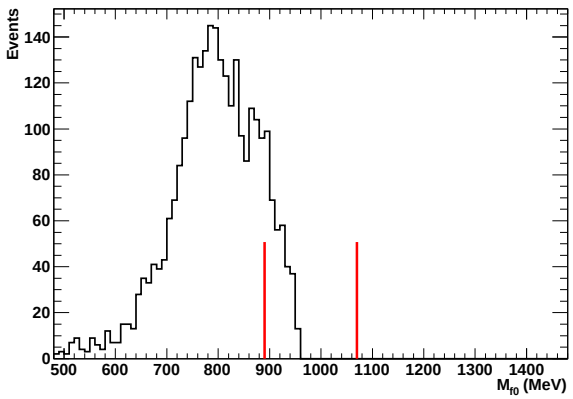

(b) $m_{\pi\pi}$

Figure 13: Distributions from $B_s^0 \to J/\psi\eta'$, $\eta' \to \rho\gamma$ decays. The vertical lines show the narrow mass windows.

4.3 Background Summary

Table 6 shows the sources of the background and expected yields from 2 fb^{-1} data. The branching fractions and b-hadron production fractions used for the calculation are shown in Table 5. The largest background arises from a J/ψ combined with random tracks identified as pions, other than $B_d^0 \to J/\psi K^{*0}$ and $B_s^0 \to J/\psi\eta'$. These backgrounds (mass shape and proper

Table 6: Summary of background sources. The numbers quoted are calculated in the narrow mass windows $|m_{\pi\pi} - m_{f_0(980)}| < 90$ MeV and $|m_{\mu\mu\pi\pi} - m_{B_s^0}| < 50$ MeV. We assume the trigger efficiencies are the same for the signal and backgrounds. The $b\bar{b}$ background does not include the specific B_s^0, B_u^+, B_d^0 channels listed here.

Sources	Yield from 2 fb^{-1} before trigger ($\times 10^3$)	B/S
signal	29.3	
background		
prompt J/ψ	3.3 ± 0.4	$(11 \pm 1)\%$
$b\bar{b}$	6.6 ± 0.5	$(21 \pm 2)\%$
$B_s^0 \to J/\psi\eta'$	0.75 ± 0.07	$(2.4 \pm 0.2)\%$
$B_u^+ \to J/\psi K^+$	1.29 ± 0.08	$(4.2 \pm 0.3)\%$
$B_d^0 \to J/\psi K^{*0}$	< 10 @90%C.L.	
Total	11.3 ± 0.6	$(39 \pm 3)\%$

time distribution) can be estimated by reconstructing J/ψ with two same sign-charged pions; we cannot use the B_s^0 mass sidebands due to reflections from specific final states. We show in Fig. 14 the $J/\psi\pi\pi$ mass distribution for like sign and opposite sign pion pairs. In the B_s^0 signal region, and even above, the distributions are in agreement.

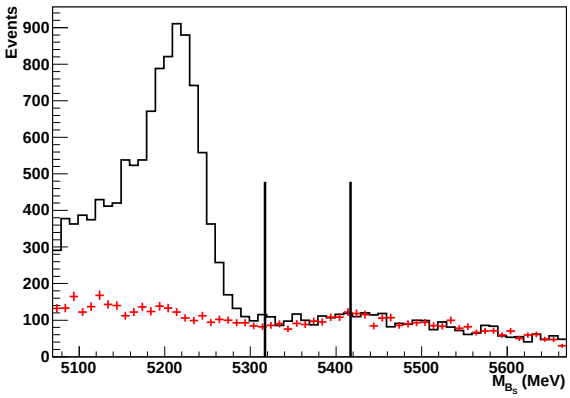

Figure 14: Invariant mass distributions from from $B_s^0 \to J/\psi\pi\pi$ candidates. The Monte Carlo sample consists of any B decay into a final state containing a J/ψ where the modes $B_s^0 \to J/\psi f_0$, $B_s^0 \to J/\psi\eta'$ and $B_d^0 \to J/\psi\pi^+\pi^-$ have been explicitly removed. The histogram is for $\pi^+\pi^-$ pairs, while the crosses represent $\pi^\pm\pi^\pm$ pairs. The vertical lines define the B_s^0 signal window .

Furthermore, as a check, we processed a 5.6 million mini-bias event sample that satisfied the L0 trigger. Only 2 events passed the off-line selection, and they both contain real J/ψ decays.

5 Properties of selected signal events

5.1 B_s^0 mass resolution

Fig. 15 shows the reconstructed B_s^0 mass distribution for the signal. Performing a double-Gaussian fit gives $\bar{\sigma}(M_{B_s^0}) = 19$ MeV, where the average width $\bar{\sigma} = \sqrt{(1-f_2)\sigma_1^2 + f_2\sigma_2^2}$, σ_1 and σ_2 are the width of the core and second Gaussian, and f_2 is the fraction of the second Gaussian [15].

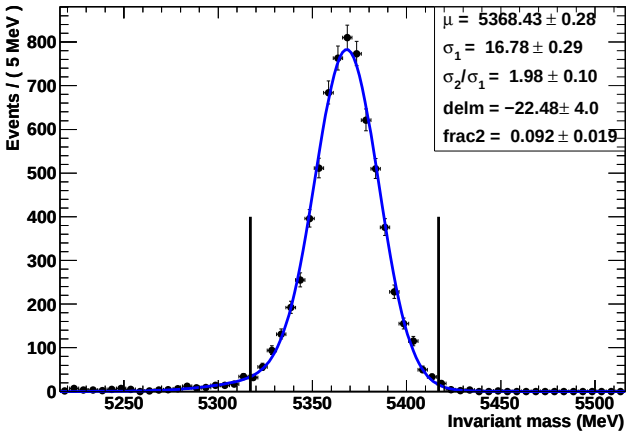

Figure 15: Reconstructed B_s^0 mass for the signal. The HLT1 trigger has been applied.

5.2 Proper time

The B_s^0 proper time is defined here as:

$$t^{\rm rec} = m \cdot \frac{\vec{d} \cdot \vec{p}}{|p|^2}, \tag{4}$$

where m is the reconstructed invariant mass, $\vec{p}$ the momentum and $\vec{d}$ the distance of flight vector of the candidate B_s^0 from the primary to the secondary vertices. If more than one primary vertex is found, the one that corresponds to the smallest IP of the B_s^0 candidate is chosen.

Fig. 16 shows the distribution of the difference of the reconstructed ($t^{\rm rec}$) and MC true ($t^{\rm MC}$) proper time. The average proper time resolution obtained from a double-Gaussian fit is 34 fs.

Fig. 17 shows the proper time error estimate and the proper time pull $\frac{t^{\rm rec}-t^{\rm MC}}{\sigma_t}$. The estimate of the error on the reconstructed B_s^0 lifetime has a mean value of 27 fs and a most probable value of 25 fs.

The time-dependent selection efficiency is shown in Fig. 18 for events before and after the trigger requirements. It is parameterized by the acceptance function defined as:

$$\epsilon_t(t) = C \times \frac{(at)^n}{1+(at)^n}, \tag{5}$$

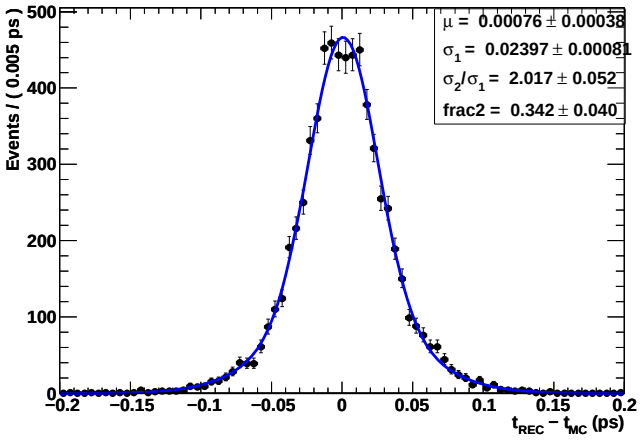

Figure 16: The distribution of the difference between the reconstructed ($t^{\rm rec}$) and MC true ($t^{\rm MC}$) proper time. The HLT1 trigger has been applied.

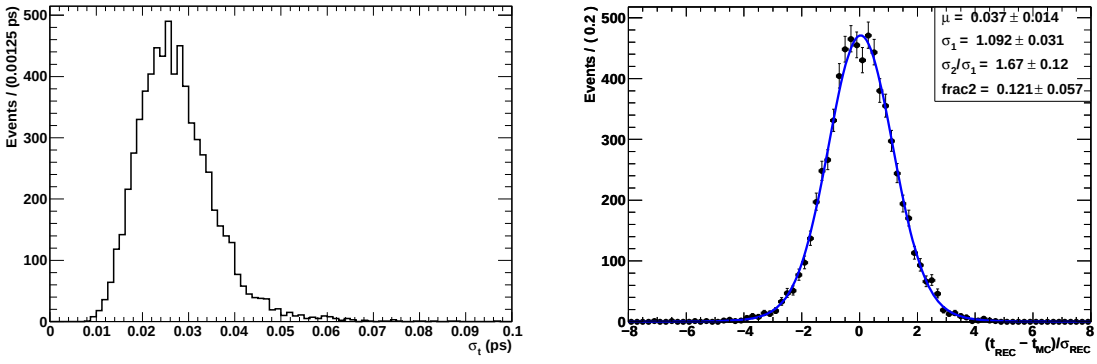

(a) σ_t (b) $\frac{t^{\rm rec}-t^{\rm MC}}{\sigma_t}$

Figure 17: Distributions of (a) the proper time error estimate and (b) the proper time pull.

where C is the selection efficiency at large decay time, and a and n are two parameters which govern the proper time dependence at small decay times.

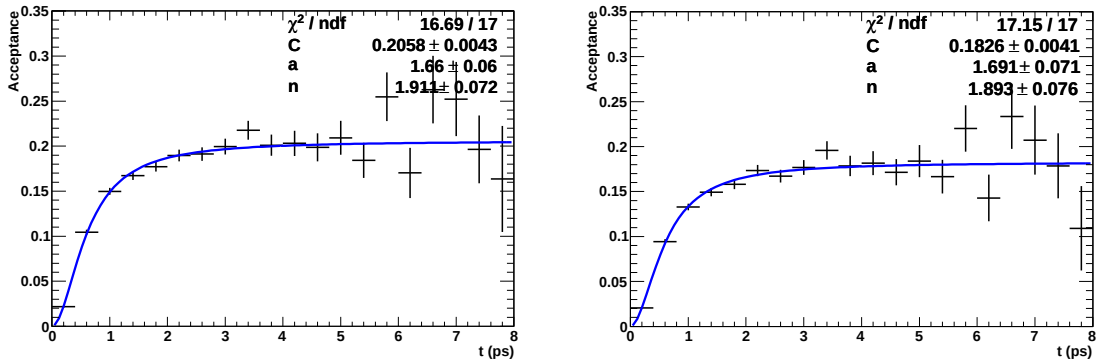

(a) untriggered (b) triggered

Figure 18: The acceptance function as function of proper time.

6 Sensitivity of $B_s^0 \to J/\psi f_0$ Compared With $J/\psi\phi$

In order to perform this task a fast (Toy) Monte Carlo simulation program has been used that is based on RooFit. We simulate 400 LHCb "experiments" with 2 fb^{-1} per sample. For each experiment the program generates events taking into account the results obtained from the full MC simulation and performs a fit according to a likelihood function which includes the $B_s^0 - \overline{B}_s^0$ mixing variables. The sensitivity to ϕ_f is taken as the root-mean-square width, σ, resulting from a Gaussian fit to the ϕ_f values from each simulation run.

6.1 Likelihood function

The time-dependent decay rates for initially pure B_s^0 or $\overline{B}_s^0$ states in $\bar{b} \to \bar{c}c\bar{s}$ or $b \to c\bar{c}s$ quark-level transitions are given by the following expressions for decay into CP eigenstates:

$$\begin{aligned}
\Gamma(B_s^0 \to f_{CP}) &\propto e^{-\Gamma_s t}\left\{\cosh\frac{\Delta\Gamma_s t}{2} - \eta_f \cos\phi_f \sinh\frac{\Delta\Gamma_s t}{2} + \eta_f \sin\phi_f \sin(\Delta m_s t)\right\} \\
\Gamma(\overline{B}_s^0 \to f_{CP}) &\propto e^{-\Gamma_s t}\left\{\cosh\frac{\Delta\Gamma_s t}{2} - \eta_f \cos\phi_f \sinh\frac{\Delta\Gamma_s t}{2} - \eta_f \sin\phi_f \sin(\Delta m_s t)\right\} \qquad (6)
\end{aligned}$$

where t is the proper time, η_f is the CP eigenvalue of the state f_{CP}, and $\Delta\Gamma_s$ is the lifetime difference between CP+ and CP– eigenstates. Direct CP violation is neglected. Note that for $J/\psi f_0$, $\eta_f = -1$.

The events are used to maximize a likelihood function ($\mathcal{L}$) which is given by

$$\mathcal{L} = \prod_i^{N_{\rm obs}} P(m_i, t_i^{\rm rec}, q_i), \qquad (7)$$

with

$$P(m_i, t_i^{\rm rec}, q_i) = f_{\rm sig} P_m^{\rm sig}(m_i) P_t^{\rm sig}(t_i^{\rm rec}, q_i) + (1 - f_{\rm sig}) P_m^{\rm bkg}(m_i) P_t^{\rm bkg}(t_i^{\rm rec}), \quad (8)$$

where:

- $P_m^{\rm sig}(m_i)$ and $P_m^{\rm bkg}(m_i)$ are the probability density functions (PDFs) describing the dependence on reconstructed mass m_i for signal and background events;
- $P_t^{\rm sig}(t_i^{\rm rec}, q_i)$ is the PDF used to describe the signal decay rates for the decay time $t_i^{\rm rec}$, which depends on the tagging result at time t=0, q_i ($q = +1$ if the signal meson is tagged as B_s^0, $q = -1$ if it is tagged as $\overline{B}_s^0$, or $q = 0$ if no tagging information);
- $P_t^{\rm bkg}(t_i^{\rm rec})$ is the PDF describing the background decay rates, which do not depend on the tagging performance.
- $f_{\rm sig}$ is the fraction of the signal in the fitting region.

The likelihood function includes distinctive contributions from the signal and the background. For both, the PDF is a production of PDFs which model the invariant mass distribution and the time-dependent decay rates. The PDF used for generating the B_s^0 mass spectrum consists of a double-Gaussian for the signal and a linear function for the background. The PDF for the proper time is modeled by a true decay function smeared by time resolution then multiplied by the decay time acceptance function. From Eq. 6, the true time decay function for the signal can be expressed as:

$$R(t, q) \propto e^{-\Gamma_s t} \left\{ \cosh \frac{\Delta\Gamma_s t}{2} + \cos\phi_f \sinh \frac{\Delta\Gamma_s t}{2} - qD \sin\phi_f \sin(\Delta m_s t) \right\}. \quad (9)$$

The effect of the wrong-tag probability $w_{\rm tag}$ is included in the dilution factor $D \equiv (1-2w_{\rm tag})$. We take this value as fixed from studies of other modes such as $B_s^0 \to D_s^- \pi^+$, and use $w_{\rm tag} = 0.334$ as our value. We take the wrong tag fractions as the same for B_s^0 and $\overline{B}_s^0$.

6.2 Input to the fast Monte Carlo simulation

The PDFs and their input parameters are shown in Table 7. The parameters of the signal are obtained from the distributions shown in Fig. 15, 16 and 18 (b). For the parameters of physics and tagging performance, we use the same as those used in $B_s^0 \to J/\psi\phi$ study [8], as shown in Table 8. The PDF of the signal proper-time is shown in Fig. 19 for both $\phi_f = -0.0368$ (SM value) and $\phi_f = -0.2$ rad, where the oscillations are apparent.

The background's proper time distribution is obtained from $B_{u,d,s} \to J/\psi X$ shown in Fig. 20. The average proper time is 1.93 ps for the signal and 1.20 ps for the $b\bar{b}$ background. We use $B/S = 0.26$ for background from b decays and $B/S = 0.05$ for that from prompt J/ψ.[3]

[3]The tagging efficiency for the prompt J/ψ background is lower than the signal and $b\bar{b}$ background [8].

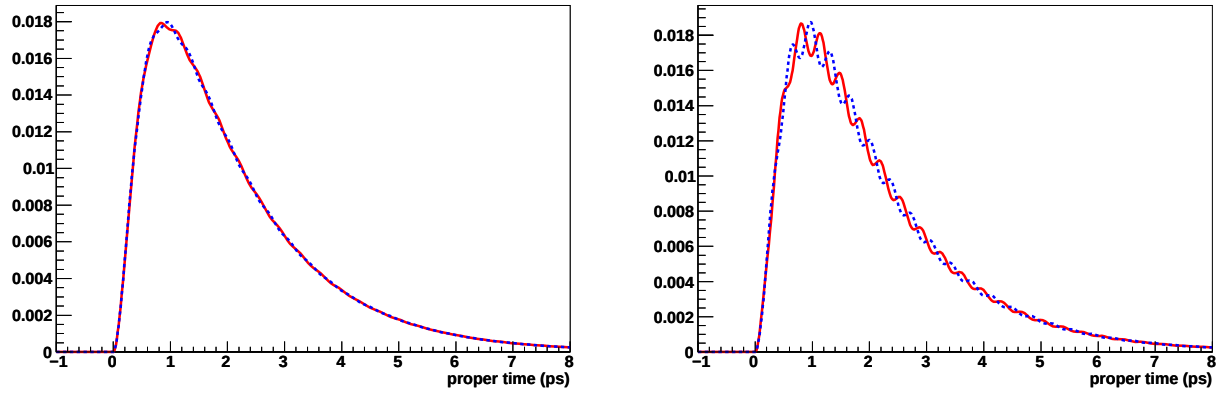

(a) $\phi_f = -0.0368$ rad

(b) $\phi_f = -0.2$ rad

Figure 19: The proper-time PDF of the signal for B_s^0 (solid line) and $\overline{B}_s^0$ (dashed line).

6.3 Fit Results

For this baseline study, we fit the Toy Monte Carlo only allowing ϕ_f and $\Delta\Gamma$ to float, with the other parameters fixed to their input values. Fig. 21 shows the distributions of mass and the proper time for the events tagged as B_s^0 and $\overline{B}_s^0$ from one experiment. The output of ϕ_f from the fits is shown in Fig. 22 with signal only and background included. The sensitivity of ϕ_f is estimated to be (0.050 ± 0.002) rad. We also find that allowing the proper time acceptance parameters to float does not increase the uncertainty of ϕ_f.

6.4 Inclusion of $B_s \to J/\psi\eta'$ Events

We have already discussed the the contribution of the $J/\psi\eta'$, $\eta' \to \rho^0\gamma$ events as a source of background in the $J/\psi f_0$ sample. We also intend to reconstruct these events when we can find the photon from the $\eta' \to \rho^0\gamma$ decay and add them into our final sample (with reversed CP to f_0 events). In our simulation we use all photons found in the electromagnetic calorimeter and those that convert in material in front of the magnet, provided that their p_T is larger than 300 MeV/c. The detection efficiency for photons in the solid angle of the detector is about 25%. In 2 fb^{-1} we estimate 5000 of such fully reconstructed events before the trigger. A previous analysis of this mode [6] concluded that an error in the measurement of ϕ_f of ± 0.8 rad could be made with a 2 fb^{-1} sample. Adding the two modes together would give an error in ϕ_f of $\pm$ 0.044 rad.

7 Systematic Errors

We have studied several sources of systematic error. Recall the outputs of our fit nominally are ϕ_f, $\Delta\Gamma$ and the time acceptance parameters (a and n). We actually determine, however, the product of the dilution D times ϕ_f and use the value of D determined from other measurements. Thus the systematic error on D is fully correlated with the systematic error on ϕ_f.

Table 7: The PDFs for the invariant mass and proper time describing the signal and background.

	P_m	P_t
Signal	Double Gaussian ($2G$) $2G(m; m_0, \delta_m, \sigma_1, \sigma_2, f_2)$ $m_0 = 5368.4$ MeV $\delta_m = -22$ MeV $\sigma_1 = 16.8$ MeV $\sigma_2 = 33.2$ MeV $f_2 = 0.09$	$[R(t^{\rm MC}, q) \otimes 2G(t^{\rm rec} - t^{\rm MC}; \mu, \sigma_1^t, \sigma_2^t, f_2^t)] \cdot \epsilon_t(t^{\rm rec}; a, n)$ $\mu = 0.0008$ ps $\sigma_1^t = 0.0236$ ps $\sigma_2^t = 0.047$ ps $f_2^t = 0.36$ $a = 1.68$ $n = 1.87$
Background from b	First-order polynomial	$[e^{\frac{-t^{\rm MC}}{\tau^{\rm bkg}}} \otimes G(t^{\rm rec} - t^{\rm MC}; \mu, \sigma_1^t)] \cdot \epsilon_t(t^{\rm rec}; a, n)$ $\mu = 0$ $\sigma_1^t = 0.039$ ps $\tau^{\rm bkg} = 0.96$ ps $a = 4.4$ $n = 2.9$
Background from prompt J/ψ	First-order polynomial	$2G(t^{\rm rec} - t^{\rm MC}; \mu, \sigma_1^t, \sigma_2^t, f_2^t) \cdot \epsilon_t(t^{\rm rec}; a, n)$ $\mu = 0$ $\sigma_1^t = 0.11$ ps $\sigma_2^t = 2.4$ ps $f_2^t = 0.17$ $a = 4.4$ $n = 2.9$

Now we will estimate the systematic error on ω_{tag}. This parameter can be measured using a combination of other modes. One simple approach is to measure ω_{tag} using $B_s^0 \to D_s^+\pi^-$. We expect differences in the value of ω_{tag} here and in the $J/\psi f_0$ mode because of different triggering in the hadronic and dimuon channels [16]. This difference can be estimated by simulation and checked using other modes. For example, we can use $B^0 \to J/\psi K^{*0}$, $K^{*0} \to K^+\pi^-$ to separately measure opposite side tagging. As input to a first estimate we decided to see the difference in Monte Carlo between the $J/\psi f_0$ and $D_s^+\pi^-$ B_s final states.

Our simulation of $B_s^0 \to J/\psi f_0$ yields $\omega_{tag} = (0.326 \pm 0.003)$, where the error is purely statistical. Using exactly the same tagging code on the mode $B_s^0 \to D_s^+\pi^-$, which of course we can and will use to measure ω_{tag}, gives a value of (0.309 ± 0.003), again the error is statistical. (We believe that we can measure ω_{tag} with excellent statistical precision, so we will ignore the statistical error.) The difference is 5.3% in ω_{tag}, or 10.6% in D. We argue that to first order we can use the Monte Carlo simulation to make the 5.3% correction to account for tagging differences between the two modes. Knowing that Monte Carlo is not perfect, we estimate that we will have $\approx 25\%$ error or $\pm 1.3\%$ uncertainty on ω_{tag} after subjecting the Monte Carlo to various tests. Thus an systematic error of 2.6% on D should be achievable without superhuman efforts. We also expect that our belief in the Monte Carlo will change with time, hopefully improving.

Two other sources of error have been investigated thus far using toy Monte Carlo. The

Parameters	Input values
Γ_s	0.680ps^{-1}
$\Delta\Gamma_s$	$0.049\ \text{ps}^{-1}$
Δm_s	17.77ps^{-1}
$\phi_f = -2\beta_s$	-0.0368 rad
ε_{tag}	0.564
ω_{tag}	0.334

Table 8: The input parameters of physics and tagging performance used for fast Monte Carlo simulation.

general procedure is that we vary a parameter, or a shape parameterization, that has been fixed in the fit by plus and minus the expected error, and then repeat the fit. We record the difference of ϕ_f output between this fit and the nominal fit. Then the distribution of the difference is used to set the error by fitting to a single Gaussian. The mean of the Gaussian is taken as the systematic error for each particular source. To check if the systematic errors depends on the central value of ϕ_f, we use both $\phi_f = -0.2$ and $\phi_f = -0.736$ for generation. We notice that the systematic error does depend on ϕ_f and σ_{ϕ_f}/ϕ_f is approximately constant. We plan to measure the time resolution in real data from prompt $J/\psi \to \mu^+\mu^-$, where we add two other tracks from the primary vertex consistent with the f_0 mass. We have seen that the pull distribution of time resolution for the signal and the prompt events, so defined, are identical. Our results are listed in Table 9.

Table 9: Systematic error sources on ϕ_f

Source	Value	σ_{ϕ_f}/ϕ_f (%)
Time resolution	34 fs varied by $\pm 5\%$	2.5
Misstag rate	0.334 ± 0.004	2.6
B_s lifetime	1.470 ± 0.027 fs	3.0
Total		4.7

These errors are of comparable sizes. They will improve with increased statistics especially in the control channels. None of the systematic errors changes our estimation of statistics necessary for a significant effect, but merely scales the value of ϕ_f. We are continuing these preliminary studies.

Other more global sources of systematic errors due to B_s production and B_s decay rates are discussed in the Conclusions.

8 Conclusions

We expect 26,100 $B_s \to J/\psi f_0$, $f_0 \to \pi^+\pi^-$ signal events in 2 fb^{-1} of accumulated LHCb data. Based on branching fraction predictions of resonant $B_s^0 \to J/\psi f_0(980)$, $f_0(980) \to \pi^+\pi^-$ and non-resonant $B_s^0 \to J/\psi\pi^+\pi^-$, where the two pions are S-wave [5], we predict an error on the measurement of the CP violating parameter ϕ_f of ± 0.050 rad. Adding in the $J/\psi\eta'$, $\eta' \to \rho\gamma$ final state that we need to measure to estimate backgrounds, reduces the error on ϕ_f to ± 0.044

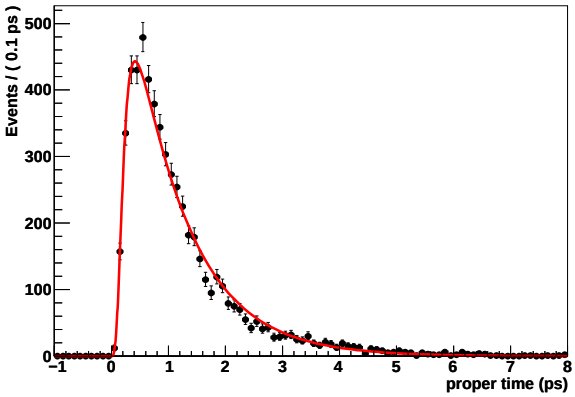

(a) background from b

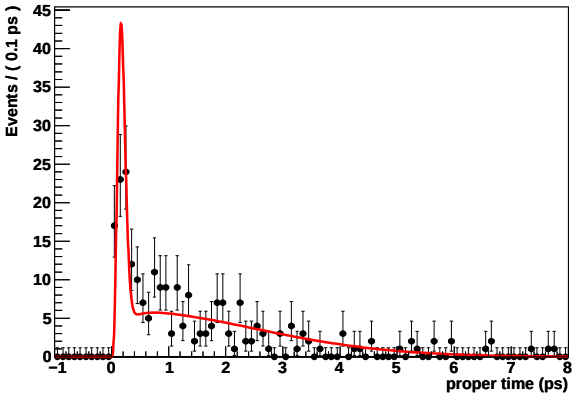

(b) background from prompt J/ψ

Figure 20: The background proper time distributions from (a) from $B_{u,d,s} \to J/\psi X$ and (b) prompt J/ψ.

rad. This is larger than the estimate using the $J/\psi\phi$ final state of ± 0.03 rad, however the latter estimate does not consider the effect of a K^+K^- S-wave. Initial indications are that taking the S-wave into account will increase the error by less than 15% [17]. Use of the J/ψ plus scalar or pseudoscalar CP eigenstates removes the need for a complicated angular analysis and should provide, at minimum, a crucial check on the vector-vector result. Both methods have a large $\approx \pm 25\%$ systematic uncertainty on the predicted sensitivity due to uncertainties in the production cross-section and B_s branching ratios. In addition, the estimate based here assumes that relative yield of the $\pi^+\pi^-$ S-wave in the f_0 mass region is 25% that of K^+K^- in the ϕ mass region. This introduces a considerable uncertainty of about $\pm 40\%$ in the relative rates and $\pm 20\%$ in the sensitivity, giving an overall uncertainty in of $\pm 32\%$ in the error in ϕ_f.

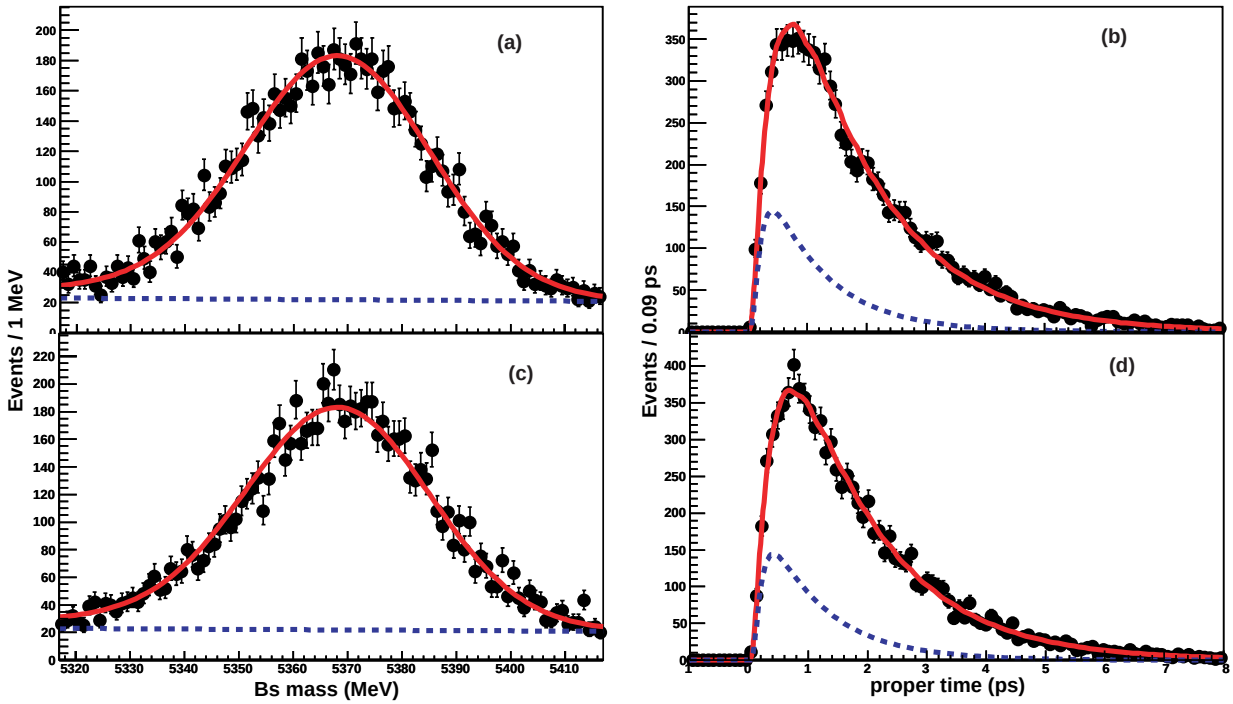

Figure 21: (a) Invariant mass and (b) proper-time distributions for the events tagged as B_s^0, and (c) invariant mass and (d) proper-time distributions for those tagged as $\overline{B}_s^0$. The points with error bars are fast simulation data and the solid lines are fit functions. The dashed lines show the background contribution.

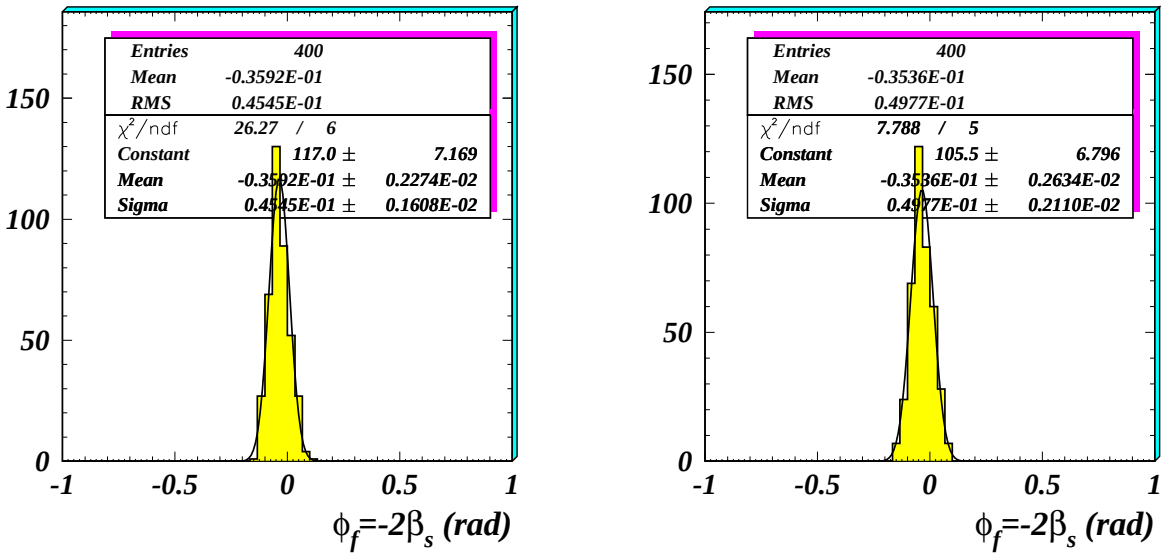

(a) signal only

(b) signal+background

Figure 22: The ϕ_f output from fitting to 400 toy MC.

9 Acknowledgments

We thank the U. S. National Science Foundation for support. We also thank our LHCb colleagues for useful discussions and review of this paper.

References

[1] Note that $\phi_s \neq -2\beta_s$, since $-2\beta_s = \arg(V_{tb}V_{ts}^*)^2/(V_{cb}V_{cs}^*)^2$, whereas ϕ_s is $\arg(M_{12}/\Gamma_{12})$, with $\arg(M_{12}) = V_{tb}V_{ts}^*)^2/(V_{cb}V_{cs}^*)^2$, and $\arg(\Gamma_{12})$ is a linear combination of $(V_{cb}V_{cs}^*)^2$, $V_{cb}V_{cs}^*V_{ub}V_{us}^*$, and $(V_{ub}V_{us}^*)^2$. See A. Lenz, Nucl. Phys. Proc. Suppl. 177-178:81-86, 2008, arXiv:0705.3802v2 [hep-ph].

[2] D. Tonelli (CDF), arXiv:0810.3229 [hep-ex]; T. Aaltonen et al. (CDF), Phys. Rev. Lett. **100**, 161802 (2008), arXiv:0712.2397 [hep-ex]. V.M. Abazov et al. (D0), Phys. Rev. Lett. **101**241801 (2008) arXiv:0802.2255 [hep-ex] and J. Ellison (D0), arXiv:0810.1041 [hep-ex].

[3] G. Punzi, "Flavour physics at the Tevatron," presented at "The 2009 Europhysics Conference on High Energy Physics," Krakow, Poland, July, 2009, to be included in the proceedings. For older results see J. Charles (CKM Fitter) `http://www.slac.stanford.edu/xorg/ckmfitter/TalkBuffer/StatusOfTheCkmMatrixCapri2008.pdf`, see also O. Deschamps (CKM Fitter) arXiv:0810.3139v1 [hep-ph].

[4] I. Dunietz, H. R. Quinn, A. Snyder, W. Toki and H. J. Lipkin, Phys. Rev. **D** 43, 2193 (1991).

[5] S. Stone and L. Zhang, Phys. Rev. D**79**, 074024 (2009) [arXiv:0812.2832].

[6] D. Volyanskyy, "Study of $B_s^0 \to J/\psi\eta'$," presented at working group July, 2007, `http://indico.cern.ch/getFile.py/access?contribId=1&resId=0&materialId=slides&confId=9609`.

[7] Other such modes previously considered include $B_s^0 \to J/\psi\eta(\gamma\gamma)$, $B_s^0 \to J/\psi\eta(\pi^+\pi^-\pi^0)$, $B_s^0 \to \eta_c(4h)\phi$, $B_s^0 \to D_s^+D_s^-$ L. Fernandez, Acta Phys. Pol B **38**, 931 (2007) [LHCb-2006-047], $B_s^0 \to J/\psi\eta'(\rho^0\gamma)$ D. Volyansky, and J. van Tilburg [CERN-LHCB-2007-027], and $B_s^0 \to J/\psi\eta'(\eta\pi^+\pi^-)$ S. Jimnez-Otero [CERN-THESIS-2007-051].

[8] J. Albrecht *et al.*, "Road map for the measurement of mixing induced CP violation in $B_s^0 \to J/\psi\phi$ at LHCb," LHCB-ROADMAP3-001.

[9] There is the possibility of an additional decay diagram involving W-exchange, where we end up with a $u\overline{u}$ system with the J/ψ being formed from additional gluons. If this diagram is significant and if the f_0 has a relatively large $u\overline{u}$ piece in its wave function, it could be a source of an additional phase. Current estimates of the light quark content in the f_0 wavefunction, however, are small, see Ref. [5] and references therein.

[10] K. M. Ecklund *et al.* (CLEO), "Study of the semileptonic decay $D_s^+ \to f_0(980)e^+\nu$ and implications for $B_s \to J/\psi f_0$," [arXiv:0907.3201].

[11] For LHCb afficinados: we use DaVinci v20r3, based on DC06 Monte Carlo.

[12] M. Calvi, *et al.* Lifetime unbiased selection of $B_s^0 \to J/\psi\phi$ and related control channels: $B^0 \to J/\psi K^{*0}$ and $B^+ \to J/\psi K^+$", LHCb-2009-025, CERN-LHCb-2009-025 (2009).

[13] C. Amsler, *et al.* (Particle Data Group), Physics Letters **B** 667, 1 (2008).

[14] K. Anikeev *et al.*, "B Physics at the Tevatron: Run II and Beyond", arXiv:hep-ph/0201071.

[15] We have not used a constraint on J/ψ mass to improve the mass resolution because of the possibilites of introducing biases. This may be implemented in the future.

[16] See M. Calvi, O. Leroy and M. Musy, "Flavour Tagging Algorithms and Performances in LHCb," LHCb-2007-058 ; CERN-LHCb-2007-058 and references therein.

[17] P. Clarke, G. Cowan, F. Muheim, Y. Xie, " Determination of $2\beta_s$ in $B_s^0 \to J/\psi K^+K^-$ Decays in the Presence of a KK S-Wave Contribution," [arXiv:0908.3627].